The Wire Flyer Towed Profiling System

CHRIS ROMAN AND DAVID S. ULLMAN

Graduate School of Oceanography, University of Rhode Island, Narragansett, Rhode Island

DAVE HEBERT

Bedford Institute of Oceanography, Fisheries and Oceans Canada, Dartmouth, Nova Scotia, Canada

STEPHEN LICHT

Department of Ocean Engineering, University of Rhode Island, Narragansett, Rhode Island

(Manuscript received 11 October 2017, in final form 5 August 2018)

ABSTRACT

The Wire Flyer towed vehicle is a new platform able to collect high-resolution water column sections. The vehicle is motivated by a desire to effectively capture spatial structures at the submesoscale. The vehicle fills a niche that is not achieved by other existing towed and repeat profiling systems. The Wire Flyer profiles up and down along a ship-towed cable autonomously using controllable wings for propulsion. At ship speeds between 2 and 5 kt (1.02–2.55 m s^{-1}), the vehicle is able to profile over prescribed depth bands down to 1000 m. The vehicle carries sensors for conductivity, temperature, depth, oxygen, turbidity, chlorophyll, pH, and oxidation reduction potential. During normal operations the vehicle is typically commanded to cover vertical regions between 300 and 400 m in height with profiles that repeat at kilometer spacing. The vertical profiling speed can be user specified up to 150 m min^{-1}. The high-density sampling capability at depths below the upper few hundred meters makes the vehicle distinct from other systems. During operations an acoustic modem is used to communicate with the vehicle to provide status information, data samples, and the ability to modify the sampling pattern. This paper provides an overview of the vehicle system, describes its operation, and presents results from several cruises.

1. Introduction

The Wire Flyer vehicle presented here is designed to provide detailed oceanographic sections in the mesopelagic region of the ocean. This region, starting below a depth of a few hundred meters, has traditionally been difficult to sample with ship-tethered and free-swimming instruments. Although there are several existing methods and instruments able to collect data in this depth range, there are still limitations to obtaining dense horizontal and vertical resolution at the submesoscale.

The most basic method for creating high-resolution hydrographic sections is repeated CTD casts in a tow-yo pattern. Doing so can create sections at any depth in the water column, but the horizontal sampling frequency is typically limited by repositioning the ship or the tow speed. Almost all CTD packages are designed for vertical use and have high-drag shapes that cause excessive wire angle when towed horizontally. This limits the effectiveness of the tow-yo approach and results in rather coarse horizontal spacing relative to good vertical resolution.

Specially designed tow bodies and fast-repeating profilers can provide denser sampling. Automated profilers, such as the Brooke Ocean moving vessel profiler (MVP) system (Herman et al. 1998; Furlong et al. 2006) and Oceanscience Underway CTD (Rudnick and Klinke 2007; Ullman and Hebert 2014), are capable of fast vertical profiling from a moving ship. These systems use specialized winches and a free-falling probe that repeatedly descends at speeds up to 4 m s^{-1}. The cycle time for the systems is determined by the cast depth, sensor fall rate, and winch speed. These systems have been successful for many applications, focusing on the upper 400 m of the water column. Repeat profiles with these systems can provide sound speed structure to thermocline

Corresponding author: Chris Roman, croman2@uri.edu

DOI: 10.1175/JTECH-D-17-0180.1

depths for multibeam sonar surveying (Beaudoin et al. 2011) and long-range acoustic propagation (Van Uffelen et al. 2010), potentially alleviating some of the need for repeated expendable bathythermograph (XBT) deployments. High-resolution vertical sections of hydrographic properties from these profiling instruments also provide insight into the mixed layer structure (Cole et al. 2010), internal waves (Ramp et al. 2012), frontal zones (Itoh et al. 2016), and submesoscale spectra (Kunze et al. 2015).

At deeper depths beyond several hundred meters, the profile rate slows and limits the along-track resolution. The Underway CTD (UCTD) can be configured to unspool the retrieval line from the winch alone, or from the winch and probe simultaneously. Spooling off the probe will increase the achievable depth but add time to the reloading and launch processes. A 400-m profile without rewinding line on the probe will typically take 15 min to repeat under normal operating conditions. Deeper casts will take longer. Data from casts down to 850 m repeating every 6 n mi (11.112 km) are shown in Hainbucher et al. (2015). During operation the probe needs to be recovered to the surface after each cast, and it is not possible to profile within a specified midwater depth band. As with CTD tow-yos, the user can adjust the ship speed to modify the profile spacing.

Detailed hydrographic sections can also be created using undulating tow bodies, such as the Chelsea SeaSoar (Allen et al. 2002), EIVA Scanfish, MacArtney Triaxus, and Sea Sciences Acrobat. These vehicles use wings to control their depth and can be towed at ship speeds up to 8 kt (1 kt = 0.5144 m s^{-1}). The limitation of these vehicles is the tow cable fixed to the body. As the vehicles profile, the tow cable is pulled up and down through the water, which creates large drag forces. This limits the vertical speed (typically 1–1.5 m s^{-1}) and the maximum operating depth the vehicles can achieve to the upper 500 m of the water column. Faired cables can help reduce the cable drag, but it is not possible to extend the towed undulating vehicle concept to greater depths. A typical profile down to 400-m depth will have a cycle time of 8–10 min and a repeat horizontal resolution of around 3 km (Pollard 1986; Rudnick and Cole 2011). At shallower depths the cycle repetition distance is reduced, but it will still be approximately 5 times the profile depth (Pichon et al. 2013; Janout et al. 2009). The benefit of towed undulated systems is the high tow speed, which can enable large surveys of hundreds of kilometers with finescale detail (Moore et al. 2007).

Sensors can also be fixed along a tow cable to improve horizontal sampling resolution. For deep sea hydrothermal plume studies, miniature autonomous plume recorders (MAPRs) have been developed (Baker and Milburn 1997; Baker and German 2004). The small units can be bolted to a tow cable and have been successful in detecting the temperature and chemical anomalies associated with hydrothermal plumes.

For CTD measurements the ADM Towed CTD-Chain uses small inductively coupled sensors and a specialized cable (Sellschopp 1997). This system provides discrete vertical resolution and nearly continuous horizontal sampling using up to 254 small individual CTD sensors attached to a tow cable. The vertical resolution can be set by the spacing between the sensors to achieve very high-resolution sections in the upper few hundred meters of the water column (Sellschopp et al. 2006). The overall specialty of the system, however, requires a dedicated coated cable and a specialized winch, and that each of the individual sensors be small and low power.

The use of gliders and autonomous underwater vehicles (AUVs) for hydrographic data collection has increased rapidly (Dickey et al. 2008; Rudnick 2016; Rudnick et al. 2018). Free-swimming gliders can profile for long durations and cover thousands of kilometers of open ocean. However, their limited forward speed (Pichon et al. 2013) makes them more appropriate for long-duration studies and less so for dynamic environments. Rudnick and Cole (2011) presents a comparison been sections collected with a glider and a SeaSoar towed profiler. The slower speed and coarser repetition pattern of the glider make it prone to aliasing time-varying features, such as internal waves. AUVs can collect large amounts of data but are not typically run in long-duration high-speed profiling patterns. The endurance of self-propelled vehicles is highly dependent on speed, which is typically less than 2 kt for extended-range platforms (Hobson et al. 2012). Additionally, the accent and descent rates of these vehicles are dictated by their trim, which is typically set to provide stable horizontal motion rather than steep pitch angles (Zhang et al. 2010). Typical vertical speeds are less than 30 m min^{-1}.

The Wire Flyer concept

The Wire Flyer vehicle was designed to provide high-resolution profiling over a specific depth band within the ocean (Fig. 1). The main difference from prior tethered profilers is that the Wire Flyer vehicle is not fixed to the end of the cable. Instead, the vehicle is autonomous and travels along the cable on rollers, which effectively separates the vehicle dynamics from the cable dynamics. The cable is essentially used as a guide for the vehicle that propels itself up and down in a controlled manner using wings. The cable drag forces are not transmitted to the vehicle and do not impede its motion. In practice the

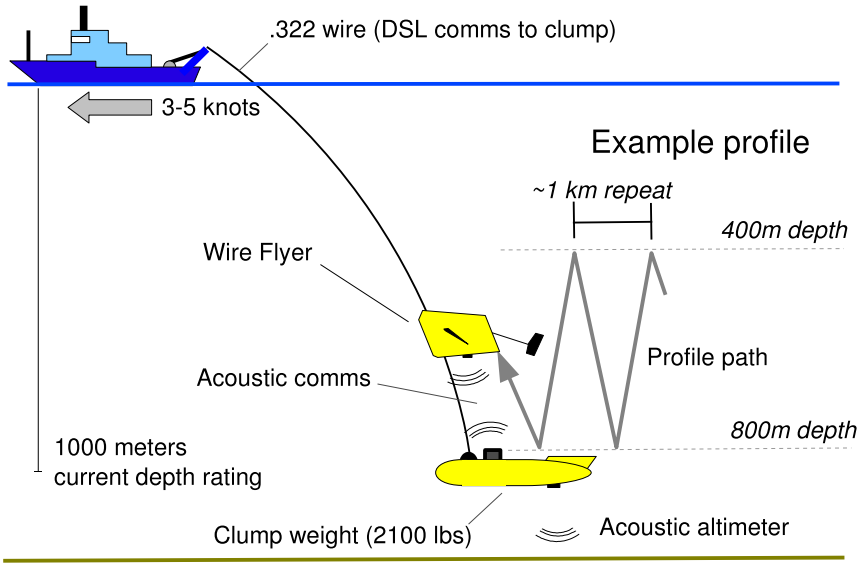

FIG. 1. Wire Flyer concept diagram showing the general operation of the system. The vehicle autonomously profiles within prescribed depth bands (e.g., 400–800 m shown here). The clump weight is attached to the cable end and is used as an acoustic communications link. The cable angle changes with depth, becoming nearly vertical at the clump and angling farther away from vertical closer to the ship.

vehicle is able to profile quickly up and down the wire at speeds up to 2.5 m s^{-1}. The shape of the cable in the water is determined by the ship speed and depth of the clump weight fixed to the end of the cable. When operating at ship speeds between 2.5 and 5 kt, the Wire Flyer can typically profile 400 m up the wire above the clump weight. At some distance above the clump weight, the wire angle will be angled sufficiently far from vertical that the achievable vertical speed will be reduced below a practical value. This typically occurs when the angle tips more than 45° from vertical and the achievable upward speed slows to less than 0.5 m s^{-1}. The current vehicle system is rated to 1000 m, but the concept is not inherently depth limited.

The remainder of this paper will provide more information on the vehicle system and present example data. Section 2 continues with a detailed discussion of the vehicle and operation. Section 3 presents some basic profiling results from several cruises and discusses the related issues of sensor and profile processing. Section 4 concludes with some summary statements and thoughts on future development work.

2. Wire Flyer system

The current Wire Flyer design (Fig. 2) is based on the successful scale model tests presented in Roman and Hebert (2011). These tests confirmed the viability of the concept and provided a sense of the performance relative to what basic modeling predicted. The two parts of the system are the Wire Flyer vehicle and the clump weight. The Wire Flyer is a streamlined shape designed to slide along the tow cable, which passes through the front of the vehicle on internal rollers. The dominant

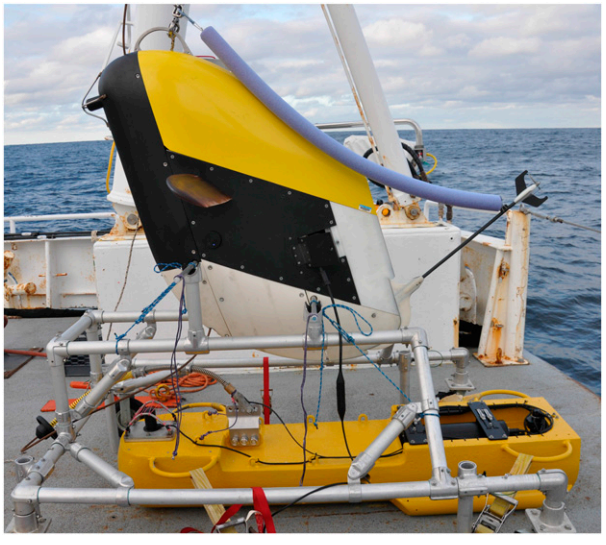

FIG. 2. Image of the Wire Flyer and clump weight on R/V *Endeavor*. The aluminum cart is used to move the vehicle around the deck. The purple foam tube is used during launch to secure the Flyer's rotating tail fin.

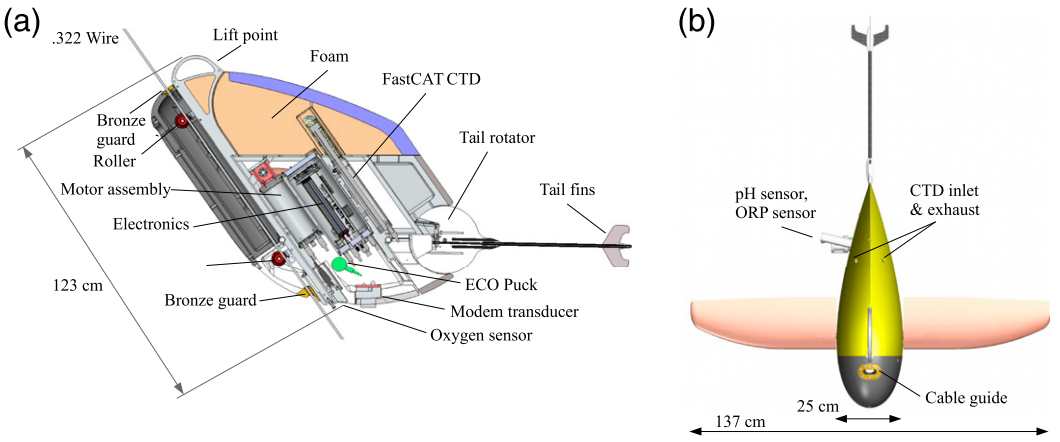

FIG. 3. Computer-aided design (CAD) images of Wire Flyer. (a) Side view section showing the arrangement of the internal parts. (b) Top view, along the direction of the cable, showing the body cross-sectional shape and wing plan.

parameters governing the vehicle performance are the body drag, wing lift, and cable angle. Towing stability and isolation from cable strum are also important factors that were initially addressed with scale testing and then refined in the full size design. The end of the cable is fixed to the clump weight. The clump is a low drag heavy weight that keeps the cable shape relatively static while towing. The clump carries the acoustic modem used to communicate with the Wire Flyer and other sensors for operations or data collection.

The following subsections provide more details on the vehicle components and design.

a. Wire Flyer vehicle

To achieve good profiling performance, the vehicle needs a low drag shape over a range of incident relative flow angles (Fig. 3). The incident flow angle will change as the vehicle travels up the cable and tips forward as the cable angle tends toward the ship. To develop the body shape, various options were tested with SolidWorks Flow Simulation (Amaral 2012). These drag values were used in numerical simulations to predict the profiling performance under various towing situations. The shape of the cable, and subsequent flow angles, were determined for various towing scenarios using the numerical cable solver WHOI Cable (Gobat and Grosenbaugh 2000). Many options for the total size and fairing shape were tried in simulation. Each body shape was evaluated at various flow angles to determine the relationship between drag and incoming flow direction. The final shape for the vehicle was chosen to have good upward climbing performance over the range of incident flow angles from 0° to 75° from horizontal. More detailed discussions of the acting forces and flow angles are presented in Roman and Hebert (2011) and Amaral (2012).

The current vehicle shape is built around a National Advisory Committee for Aeronautics (NACA) 0025 wing section. That section is extruded to make the main volume of the vehicle. The top is rounded and sized for the volume of flotation needed to offset the weight of the components. The bottom is narrower and faired to reduce drag when traveling in the upward direction, when the speed through the water is highest.

To help maintain stability while towing, a tail fin is used. The fin assembly is fabricated in lightweight carbon fiber and rotates to align with the flow in a low drag position behind the vehicle. A tilt sensor is mounted on the assembly to measure the angle of the tail relative to the body. Initially, a small propeller and shaft were mounted on the end of the tail, and an encoder was used to measure the propeller's rotational speed. Unfortunately, since the tail propeller is in the wake of the vehicle, determining the relationship between the propeller rotations and vehicle speed is more complicated than a single scalar conversion factor. Currently, the vehicle is operated without the tail propeller and the control system (section 2d) uses the tilt sensor for a measure of incoming flow angle instead.

The vehicle captures the wire using two rollers inside the front fairing. The rollers are attached to the frame using U-shaped mounts that allow the wire to be slipped in from the side and remain captured behind the rollers. The current rollers are made of urethane with a 90 Shore A hardness. The rollers have a parabolic-shaped groove in them to allow the wire some lateral movement but keep the wire tracking toward the center of the roller. This freedom allows the wire to strum rather than to try to remove the wire motion. The wire passes through slots in the fairings on the top and bottom of the vehicle.

The slots are ~6 cm in width, and also allow the cable to strum freely. The urethane rollers are the second iteration. The original rollers were made of acrylonitrile butadiene styrene (ABS) plastic with a narrow groove. These rollers were allowed to slide laterally several centimeters on the shaft. Conical springs were used to dampen the motion and to keep the rollers from contacting the bracket. This design led to spring fatigue failure and roller wear within a 100 km of travel up and down the wire. The urethane rollers have no springs to fatigue and show minimal wear after many hundreds of kilometers of wire travel. Thus far, the vehicle has used 0.322 CTD wire and simple 5/16-in. (~8 mm) trawl wire. By adjusting the roller and slot sizes, other wire sizes could be handled easily.

The top of the vehicle is made of machined syntactic foam. The overall buoyancy of the vehicle is slightly positive [<5 lb (2.3 kg)] and is set with lead ballast pieces. The small amount of flotation allows the vehicle to float up the wire should the ship stop and the vehicle lose wing lift. The buoyancy seems to have little effect on the achievable profiling performance of the vehicle, as the hydrodynamic drag and lift forces dominate the buoyancy forces when towing.

The wings are constructed as a modified NACA 0018 section, which is known to have good lift characteristics and is tolerant to stall at high angles of attack. The wings are 56 cm long and have a chord length of 19 cm. The inner 22 cm of the wings are a straight extrusion and the remaining part tapers at the leading edge (Fig. 4). This was done to reduce the tip vorticity and also shed potential debris from the wing. The internal structure of the wing is made of aluminum stiffeners connected with fiberglass rods. The wings are cast from a urethane with a 60 Shore D hardness. This material has enough stiffness for the wing load but is durable enough to withstand some abuse during shipboard handling. The wing shafts are sized for a nominal peak wing force of 1000 N, which could be generated at high speeds and optimal trim angles.

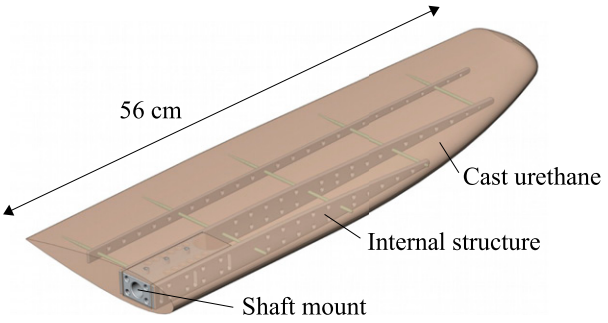

FIG. 4. CAD image of a urethane molded wing.

1) ELECTRONICS

The main electronics for the vehicle are contained in a 1000-m-rated pressure housing. This includes the computing, batteries, power switching, acoustic modem, and sensor communication electronics. The computer is a Gumstix Advanced RISC Machines (ARM) processor running Ubuntu Linux. The batteries are Inspired Energy rechargeable lithium-ion cells, with a total 380-W capacity. These provide the vehicle with a nominal 24-h running endurance. The average hotel power draw is typically 12–15 W with the typical CTD, oxygen, and fluorometer sensor suite. The instantaneous power, however, varies depending on the wing motor and acoustic modem. The motor typically draws 5 W to hold the wings at a relatively constant angle, but it will draw 30 W when sweeping the wing angle during a turn. The modem will draw 50 W for a few seconds during a transmission. The wings are driven by an Animatics SM17205D SmartMotor and bevel gear connection. The SmartMotor contains its own internal processor and local digital inputs. The motor is able to run small programs for the wing angle calibration and position limits, and also has a software deadman routine that will return the wings to an upward angle should communications to the main computer be lost. There is a breakaway mechanical clutch between the motor and wings. This allows the wing shaft to break free and rotate without damaging the motor or gearing should the wings impact something while operating or strike the ship during a recovery. The wings can be spun manually to reengage the clutch.

2) SENSORS

The vehicle carries several sensors. The central instrument is a 16-Hz Sea-Bird 49 FastCAT CTD sensor. This unit is pumped with tube connection to the outside through the top of the foam flotation. The inlet and exhaust tubes are symmetric relative to the vehicle centerline to avoid any pressure differential caused by the flow around the vehicle. The head of the sensor is in a partially sealed volume cut into the foam that is continuously flushed by a small brushless aquarium pump. The flushing helps keep the sensor head bathed with water similar in temperature to the water outside the vehicle. This reduces the thermal lag in the temperature measurement. In general, there will be a difference between the internal and external temperatures because of the vehicle traveling through vertical temperature gradients and the low flushing rate of water through the inside of the vehicle. More details regarding the sensor data processing are given in section 3b.

The Flyer also carries an Anderraa 4831F oxygen sensor; a Wetlabs Triplet Ecopuck for measuring turbidity, chlorophyll, and colored dissolved organic matter

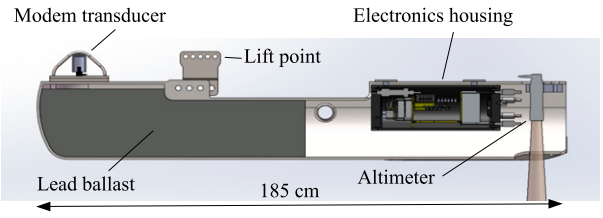

FIG. 5. CAD image of the clump weight.

(CDOM); and a Sea-Bird 27 pH/ oxidation reduction potential (ORP) sensor. These sensors are mounted with the measurement faces outside the vehicle in the free flow. Sensor sample plots are show in section 3c.

b. *Clump weight*

The clump weight is a ~950-kg tow body made of steel and lead (Fig. 5). It is approximately 185 cm long and 41 cm in diameter. It contains a 2000-m-rated electronics housing for the acoustic modem, pressure sensor, and basic electronics for power and digital subscriber line (DSL) communications over the tow cable. The 2000-m rating on the housing is needed because more than 1000 m of tow wire are required to operate below ~700-m depth as a result of the cable layback. In the event of a ship failure, the housing should be able to withstand the wire hanging straight down. An external Tritech altimeter is mounted in the aft end of the clump to determine the distance to the bottom. An Esmet wire termination is used on top of the clump along with a 1-m-long spring assembly. The spring is a progressive stiffness motorcycle suspension part and is used to soften an impact should the Flyer run into the clump during operations.

c. *Operations*

The components and interconnections of the Wire Flyer system are shown in Fig. 6. The system can be operated using standard 0.322 oceanography wire with two or three electrical conductors. A 350-V dc power supply is used to power the clump though a DSL modem box. The system has also been run in shallow water (30 m deep) off a 13-m vessel using a trawl wire and simple lead weight instead of the clump. During normal operations two computers are generally used. The main topside computer runs the software for the clump sensors, handles the acoustic modem communications, and records data from the ship. A second computer is used to run the Flyer–graphical user interface (GUI) interface, look at data, and send updated missions to the vehicle via the modem.

The software for the Wire Flyer is written in both C and Python, and utilizes the Lightweight Communications and Marshalling (LCM) library (Huang et al. 2010)

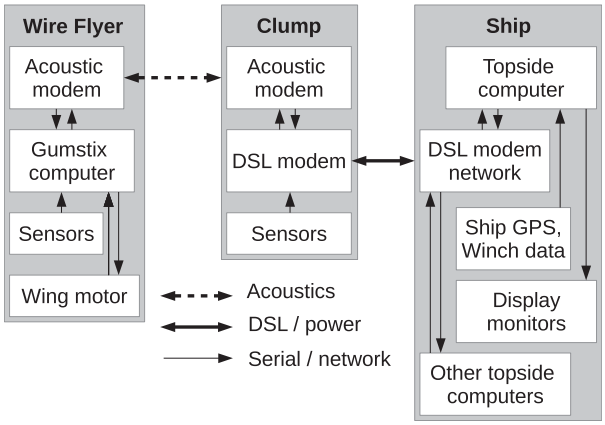

FIG. 6. An overview of the Wire Flyer system components and data connections.

for communications between individual programs and logging. The LCM framework allows the operating software to be broken into a collection of small asynchronous single-purpose programs that exchange data via network messages over the user datagram protocol (UDP) protocol. This allows for easy implementation of sensor drivers, control code, and mission execution. The system also allows for easy logging of data messages and faster than real-time simulation of a mission using all of the operational software. The sensor data are recorded at each sensor's individual output rate on the Flyer's onboard computer using the standard LCM logger. The logger listens to the LCM message traffic produced by the sensor drivers and writes the data messages to a binary file. This file can be parsed after a deployment to produce log files for MATLAB or general CSV files. The binary log files can also be replayed to broadcast the recorded data messages back to the operating software. This is useful for debugging and testing new software features offline. The control and mission management programs run a regular 10-Hz loop and also generate messages for the LCM logger.

1) ACOUSTIC COMMUNICATIONS

A WHOI micromodem is used to communicate between the Flyer and operators station on the ship. The operator-side modem is mounted to the clump to exploit the fact that the clump and vehicle are far removed from ship noise and so it typically experiences more robust communications than would be the case using a hull-mounted transducer. In practice the communications are generally reliable when the depth difference between the Flyer and the clump is less than 400 m. A separate ship-towed transducer can be used as a backup if needed. The modem is used to receive status updates and data from the Flyer, and to send updated mission

commands. Regular status messages are broadcast using 256-byte acoustic packets every 30 s in a repeating cycle. The messages contain basic vehicle information (e.g., the present depth, wing angle, vertical speed, mission time, status information, CTD data) and a short buffer of depths over the last minute. This short depth history is used to plot out the profile path with some robustness to missed messages. The ship-side modem starts the communications cycle by sending a ''request for status'' message to the Flyer. This request contains the current clump depth. The Flyer maintains an estimate of the clump depth and can use it to adjust the turnaround depth at the bottom of a profile. The Flyer will make the bottom turn at the desired mission depth or at a set distance above the clump depth, whichever is shallower. This avoids potential collisions between the vehicle and clump should the clump come up shallower than the Flyer's intended mission plan. If the Flyer does not hear any request-for-status messages for a preset timeout, the Flyer modem will start to send acoustic-range-only pings to the clump. These will return the range to the clump and will also be used to update the Flyer's clump depth estimate. This is a safety fallback should the ship lose communications with the clump over the DSL modem or the software driver for the clump modem crash. The response for a range-only request is answered by the clump modem in hardware directly, and it will work as long as the modem has power. A second timeout is set to trigger a vehicle abort if the range requests are not answered. Should this occur, the safe way to recover the system is to slow the ship down and allow the clump weight to drop and the vehicle to float up the wire. In doing so there is little chance for the clump and vehicle to collide.

The Flyer modem driver also keeps configurable buffers of subsampled sensor data that can be requested in dedicated acoustic data messages. For example, a 2048-byte buffer can be set to hold the most recent 250 oxygen–depth measurement pairs, each 1-s apart. These data messages can be requested at any time by the topside interface. The returned data are plotted in the user interface and interlaced with the sparse points returned by the regular 30-s status updates. This allows the operator to create a preliminary down-sampled view of the full-resolution data stored on the Flyer and is helpful in potentially updating the current mission over the acoustic link. New mission files can be parsed, compressed into a command string, and sent over the modem. The vehicle will receive the message and update the current mission plan. New plans can be appended to the current mission or start a new sequence of behaviors. A simple ''abort'' command can also be sent to stop the current mission and return the vehicle to the surface for recovery. New missions can also be sent to the operator's Flyer-GUI user interface to update the anticipated depth trajectory.

2) FLYER-GUI AND CLUMP-GUI

During operations the Flyer-GUI program (Fig. 7) displays the data received from the Flyer modem in a graphical interface. The display shows the current status message, plots the depth history, shows the anticipated future mission plan, and displays data plots from prior status messages or full data messages. The program is written in Python and receives data via LCM messages over the network. Any number of GUI instances can be run by shipboard computers on the local network, each of which controls its own viewing interface to display data received via the LCM messages. A simpler Clump-GUI program is run as a winch operator display. It shows the Flyer depth history, future mission plan, and the clump depth history. It is typically routed to a monitor located at the winch operator station. The clump is typically towed 10–15 m deeper than the bottom profiling depth of the Flyer. If the clump comes closer to the Flyer, a warning will alert the winch operator. The clump altimeter data are similarly displayed when operating near the bottom.

3) MISSION PLANNING

While operating, the mission management software running on the Flyer executes the user-specified profiling pattern, monitors for any fault conditions, and responds to external inputs from the acoustic modem link. Sample dives showing different profile patterns are shown in Fig. 8. The specific depths, speeds, and timing of the profiling sections are specified in a mission script. An example script is given in appendix A.

Customized profile patterns, such as a step profile (Fig. 9), can also be implemented and executed with excellent repeatability. The stairstep was used to investigate the time constant associated with the oxygen sensor.

Fault conditions, such as low battery or the loss of sensor data, will cause the vehicle to abort the mission and return to the surface with the wings at a fixed upward angle.

d. Control system

The vehicle operates with a closed-loop control system that actively changes the wing angle to achieve the desired depth or velocity profiles. The control system requires knowledge of the vehicle's depth, from the CTD sensor; the tilt angle of the wire; and the current position of the wings. The wire tilt is measured with a tilt sensor mounted in the electronics housing. The wing

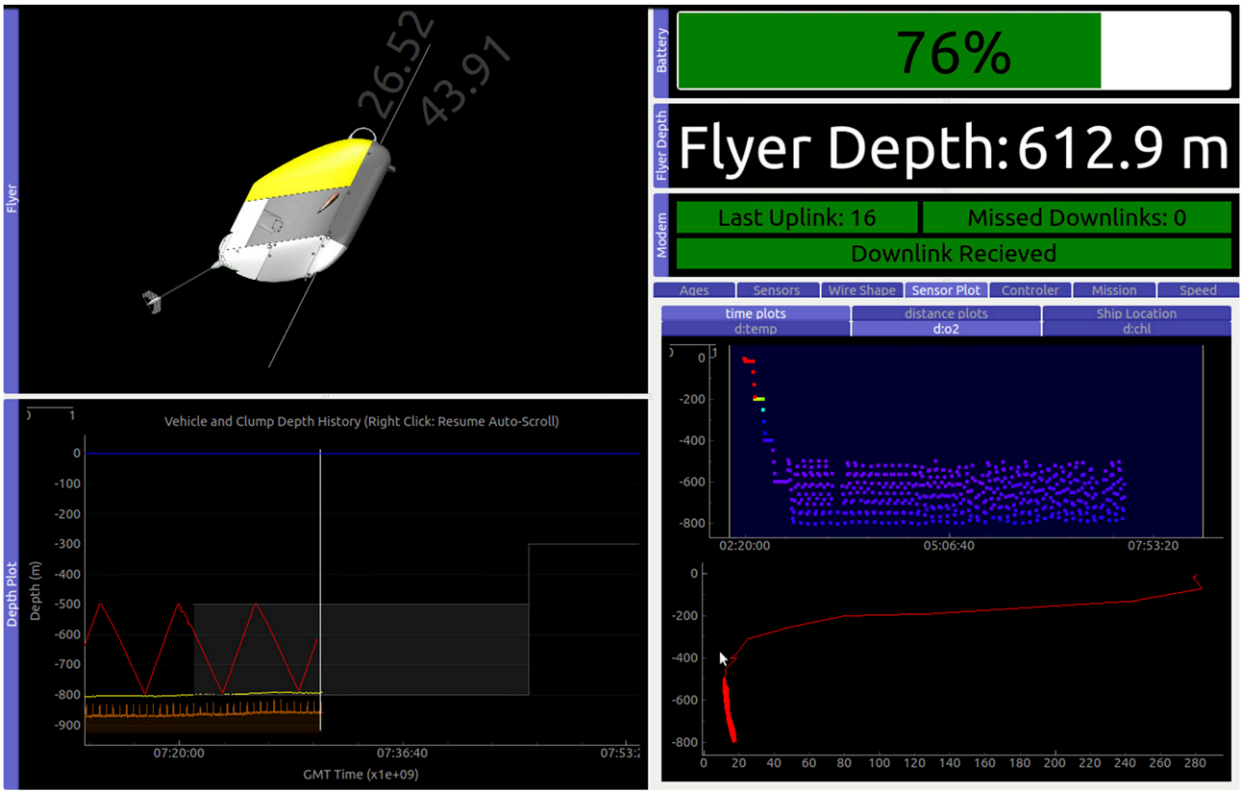

FIG. 7. Screen capture of the Flyer–GUI operational program. (top left) The vehicle tilt, tail, and wing angles. (top right) The depth, modem timing, and battery capacity. (bottom left) A scrollable time plot showing the Flyer depth history and the anticipated future sampling window in gray. (bottom right) Sensor data plotted as a scrolling time/depth plot. The tabs show additional sensor plots and status information.

angle is known from the position-controlled motor and encoder. The wing rotation is always referenced to a known position, indicated with an infrared limit switch inside the motor housing. New position commands are sent to the motor at 5 Hz. The control system is a conventional proportional integral derivative (PID) controller. Some additional features are used to account for wing stall and to improve the velocity tracking performance through the turns at the top and bottom of the profiles. Some example velocity profiles are shown in Fig. 10.

On upward profiles the vehicle is generally able to reach the desired speed for the majority of the profile, but it may reduce speed near the top of a profile. As the cable angle tips farther from vertical, the projection of wing lift forcing up the cable is decreased and the projection of the vehicle's drag forcing down the cable will increase. This will lead to a loss of speed and potentially to a point where the forces along the cable balance and the vehicle stops moving. The vehicle can also stop if a stall condition occurs, where the wing lift force is dramatically reduced because of flow separation.

On downward profiles the vehicle typically starts off slowly and increases speed as it descends. Near the top of the profile, the vehicle tends to lose apparent velocity through the water, which reduces the lift force on the wings. This occurs where the cable angle causes the vehicle to slide backward and down relative to the ship, decreasing the through-water speed. As the vehicle descends, the wire angle at the vehicle becomes increasingly vertical, which increases the apparent velocity and downward wing force. This allows the vehicle to speed up and eventually reach the desired downward velocity. The free-body diagram explaining all of the relevant forces and angle conventions is shown in Roman and Hebert (2011). A more complete summary of the achievable profiling performance is provided in Logan (2014), which looks at the results from the first test cruises and makes comparisons to the performance predictions and simulations.

Stall occurs when the angle of attack, the difference between the wing angle and the incoming flow angle, becomes too large. The standard PID controller will increase the wing angle to increase the profiling speed if the vehicle is traveling too slowly. This can eventually

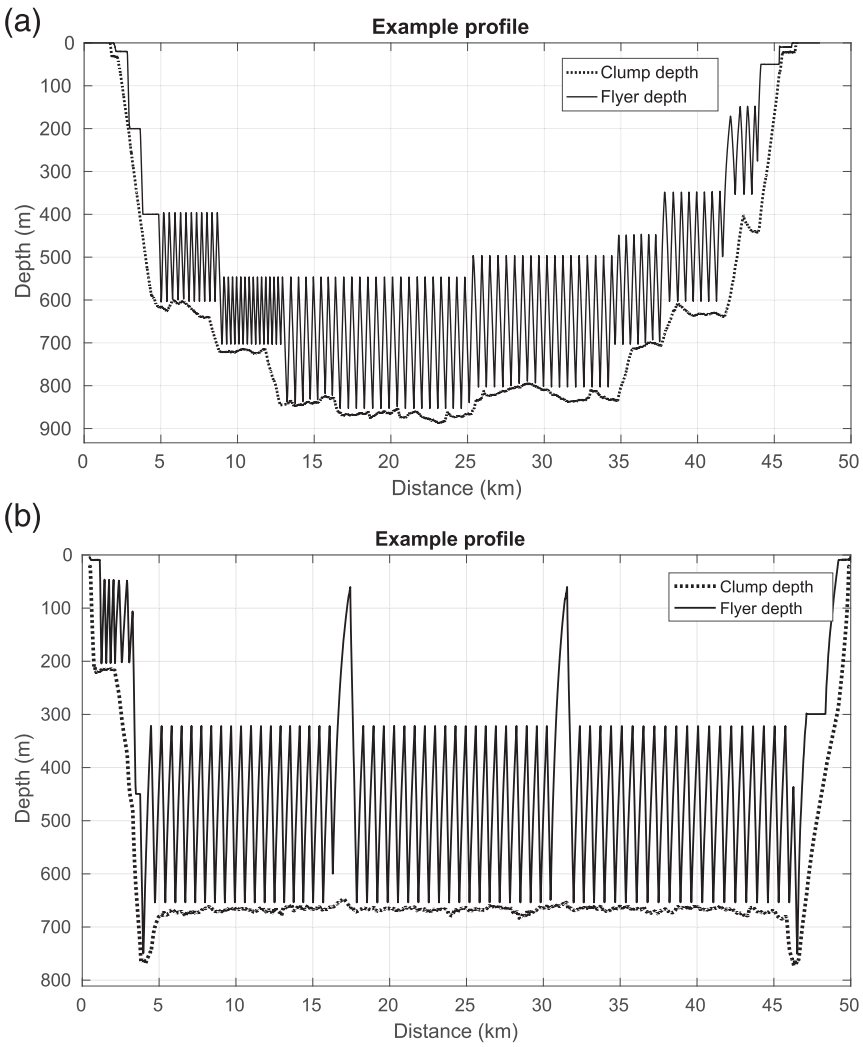

FIG. 8. Example profile patterns. (a) An 8.5-h dive showing the Wire Flyer profiling in various depth bands. The bottom of some profiles show the vehicle corrected for the clump rising into the desired depth band and the vehicle turning around at a shallower depth. (b) A mostly regular pattern with deeper and shallower excursions.

drive the wings into a stall condition near the top of a profile. As the vehicle travels up the cable and tilts forward, maintaining the upward profile speed becomes more difficult as the vehicle is moving both up and forward toward the ship, against the relative horizontal flow. For sailors, the analogy is sailing progressively closer to the wind to the point of pinching, where speed is lost. At some point increasing the wing angle is not helpful and will not increase the vehicle speed. At the stall point, the wings will lose lift and the vehicle will eventually stop moving along the cable. To counter this behavior, the control system uses the tilt sensor located on the rotating tail to measure the angle of the incoming flow. A stall limit is implemented to stop the wings at a maximum angle of attack. When the limit is reached, the angle of attack will remain constant even as the vehicle tilt angle changes. In this condition the vehicle may not be able to track the desired upward velocity, but it will always make upward progress and not stop moving along the wire (Fig. 11). In practice, stall limits of 15°–20° have proven to be effective.

To improve the performance in turns, an adaptive approach is used. The adaptive control term will record the wing angle when the vehicle first achieves its desired up or down speed during a profile cycle. The wings are then driven toward this angle using a feed-forward term during the next top or bottom turn. The effect is improved performance in the turns that stabilizes within a few initial cycles after a pattern change (Fig. 12). This

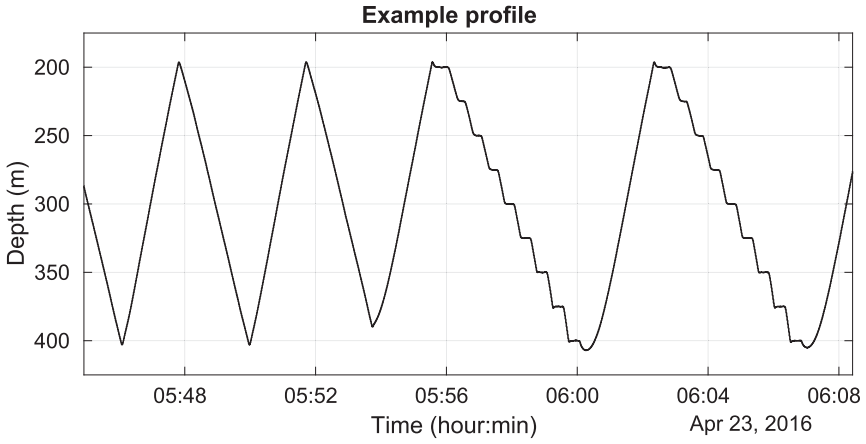

FIG. 9. A step profile that pauses briefly at equal depth increments during the descent.

approach allows the basic PID controller to be tuned to achieve the steady profiling velocity while retaining quickness in the up/down transitions. Since the vehicle typically completes tens or hundreds of cycles in a deployment, adapting the performance over the first couple of cycles is very reasonable.

e. *Launch and recovery*

The Wire Flyer is typically launched through an A-frame (Fig. 13). The basic steps begin by lifting the Flyer from the deck into a custom sheave with integral sway limiting supports. This is done with a lift line that is routed through an extension spring tensioner on deck and a pneumatic tugger. The Flyer is held steady in the sheave between two arms. The extension springs provide the necessary compliance for the Flyer to be held in the sheave as the A-frame moves in or out. The second step is to deploy the clump weight and lower it down to ~20-m depth. The wire will slide though the Flyer freely while it is held in the sheave. The third step is to lower the Flyer into the water and release it. The Flyer then waits a few seconds on the surface before moving to a constant preprogrammed depth, typically 10 m. This depth puts the vehicle below the propeller wash and wave surge, and safely above the clump. While the vehicle is holding depth, the clump weight is lowered below the Flyer's planned pattern. When working below 500-m depth, it can be helpful to use a few intermediate depth steps for the Flyer to maintain acoustic communications with the clump as it is lowered. During this

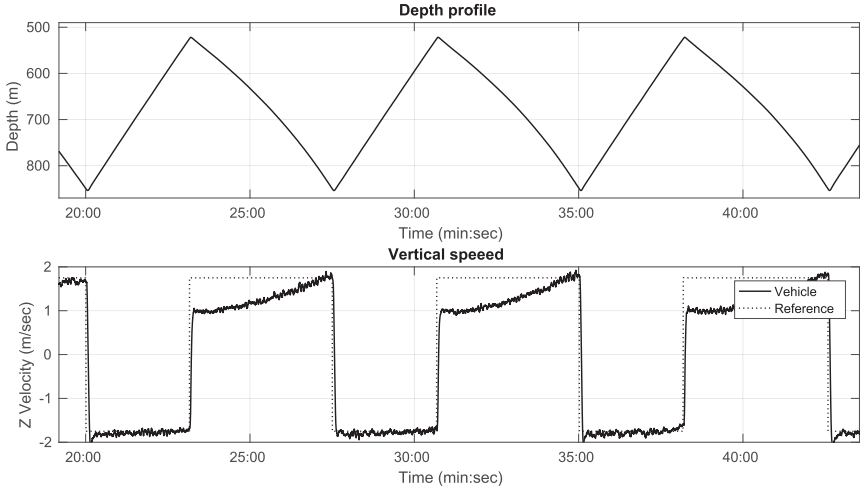

FIG. 10. Sample profiles showing the vehicle depth and velocity. The upward profiles are able to obtain the desired speed over the depth range. The downward profiles start slower at the top and increase speed to the desired amount on the way down. Note that the depth sign convention is positive down.

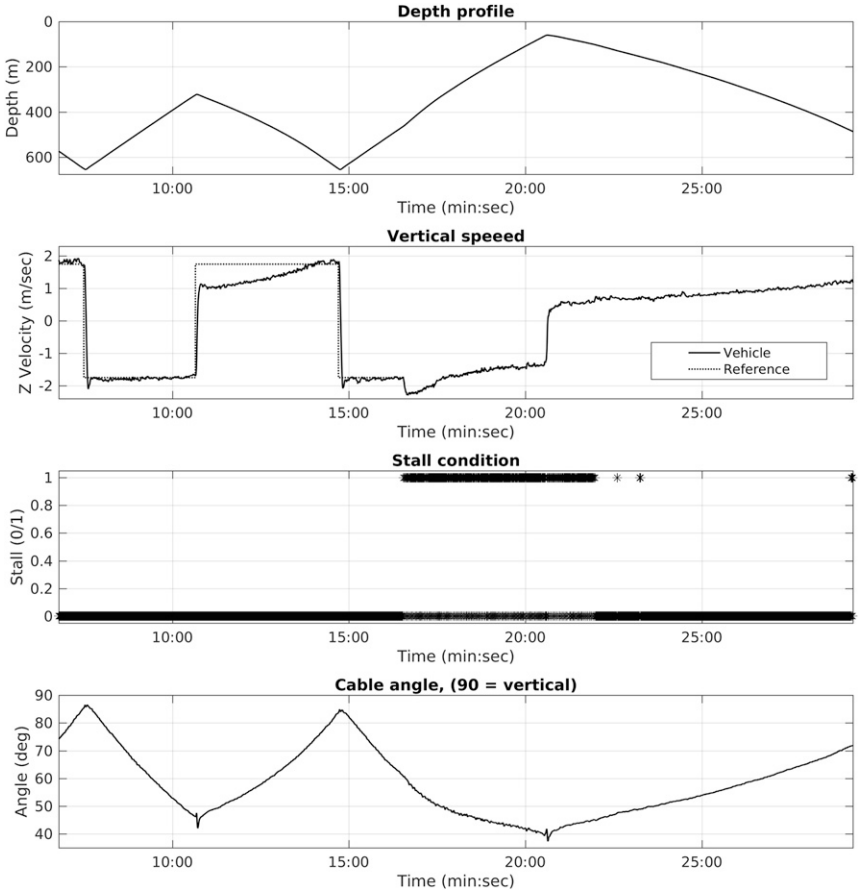

FIG. 11. A sample profile showing the stall compensation. Here the vehicle breaks out of a 350–650-m profile section to climb through the thermocline to 50-m depth. As the vehicle ascends the cable, the angle gets farther from vertical and the wings start to enter stall. When the stall condition is flagged (flickering between 0 and 1), the wing angle is adjusted to keep the angle of attack constant at the stall limit. In this situation the vehicle loses some upward speed, but it is able to move upward even when the cable angle is 50° from vertical.

process the ship will maintain ~2 kt through the water before eventually coming to the desired towing speed in the range of 2–5 kt. Depending on the depth and currents, the ship speed can be varied to maintain an optimal cable angle such that the Flyer is able to climb to the top of the desired profile pattern without losing speed. An operator watching the Flyer-GUI interface can see the cable angle and vehicle speed, and provide instructions to the ship. The Flyer is recovered by reversing these steps. The Flyer has been operated numerous times in sea states of Beaufort 5 or 6. In these sea states, handling the clump weigh safely is the primary concern. It is worth noting that ship heave does not affect the profiling behavior of the Flyer. The wire slides though the vehicle and the vehicle is not directly tugged by the wire. The system has also been deployed off the side of a ship using a crane boom. The same basic launch and recovery steps are used in this case.

3. Field results

The Flyer system has been used on a several cruises and has spent hundreds of hours operating. The first deployments were used to evaluate the performance of the vehicle against the initial predictions and model tests. The deployments have now transitioned to science operations and improving the capabilities for real-time evaluation of the data while the vehicle is running. Postprocessing data involves computing the actual vehicle position behind the ship and then creating depth sections that account for the vehicle location, depth, and the time response of the sensors.

a. Cable layback

The cable shape will affect the exact position of the Wire Flyer behind the ship as it is being towed. The ship's GPS location while towing is recorded, and

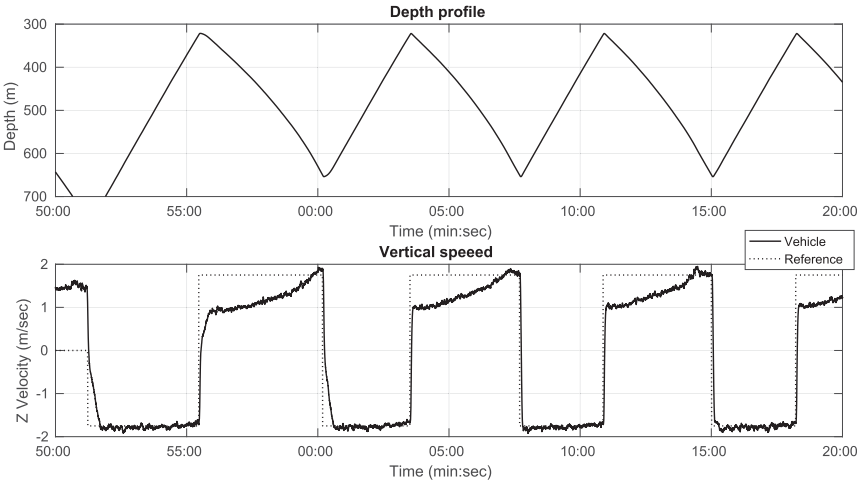

FIG. 12. Profile plot showing the adaptive wing angle feed-forward control improving the velocity control performance in the turns. The actual velocity follows the intending velocity near the transitions more closely after a few cycles.

the vehicle's position is extrapolated behind the ship using the ship's prior track and an estimate of the cable layback at the Flyer's depth. Cable shape can be predicted using numerical simulations (Gobat and Grosenbaugh 2000), but this is not practical for assessing the layback at any given time utilizing measurements of the vehicle depth, cable length, clump depth, and vehicle tilt. When plotted against depth, the vehicle tilt measurement (which is a good proxy for the cable angle) has a linear trend (Fig. 14).

This linear relation is exploited in an iterative method, described in appendix B, to solve for the layback distance at any time during the deployment using the measured cable length as a constraint. Figure 15a shows how the length-constrained linear approximation matches the measured cable angle. Although there is some separation between the angle measurements and the linear fit, the solution is generally well behaved, honors the measured cable length, and provides an angle estimate for the whole length of the cable. In general, the cable shape changes slowly, over minutes or longer, and this prediction works well over the course of a deployment. The variability over time is caused by changes in ship speed and water column currents that necessitate more or less cable length to keep the clump weight at a constant depth. Other solutions that have tried to incorporate direct cable angle measurements where the vehicle is operating have been less robust and difficult to constrain by the measured length. Figure 15b shows a layback estimate for an entire dive.

The actual vehicle position at each point in time is assigned by finding the ship's prior GPS position that is the layback distance back along the actual ship path. After correcting for layback, the vehicle's actual trajectory through the water shows it moving more horizontally through the water toward the ship on the accents and then falling more vertically during the

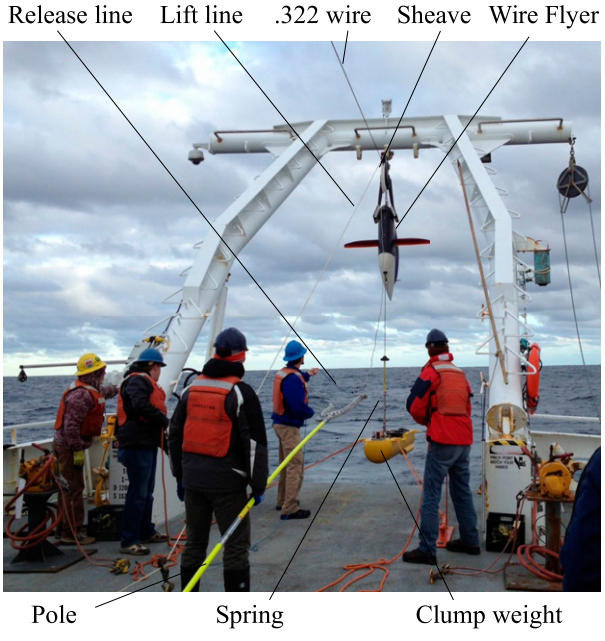

FIG. 13. Launching the Wire Flyer. The vehicle is shown in the sheave as the clump weight is deployed over the stern. The extension springs (out of frame) on the lift line keep the Flyer snug in the sheave without the danger of snapping the lift line when the A-frame moves. A custom pole is used to steady the vehicle as it is lowered from the sheave to the water. A release shackle with a trigger line frees the vehicle once it is in the water.

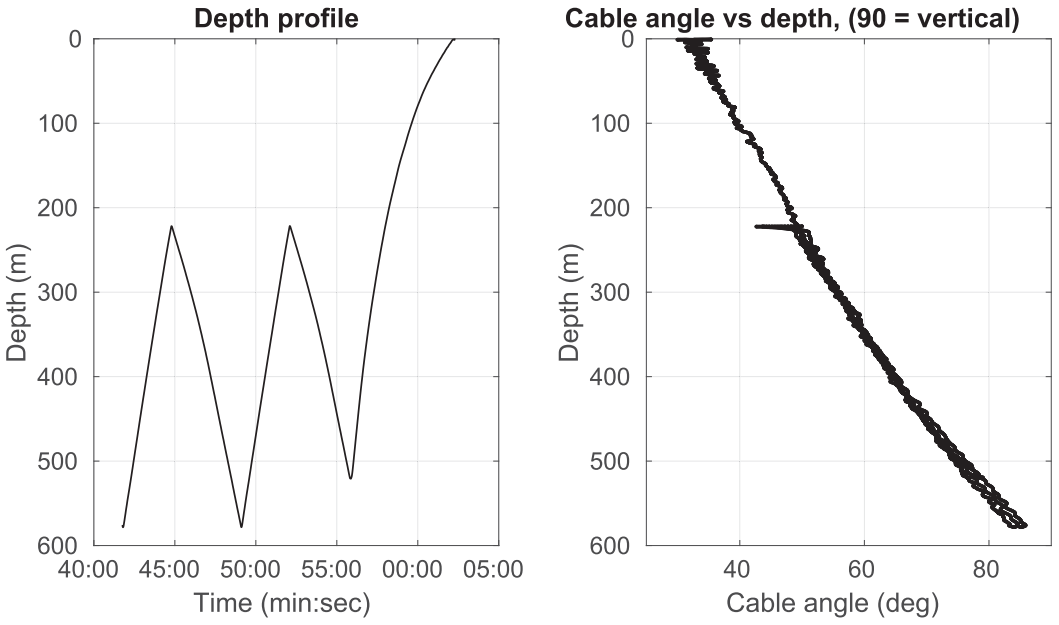

FIG. 14. Measurement of cable angle as a function of depth. (left) Vehicle profiles at depth followed by the vehicle ascending to the surface on a constant cable shape. (right) A scatterplot of the cable angle as a function of depth is nearly linear.

descents (Fig. 16). Profile cycles nominally repeat at a distance that is roughly twice the vertical depth range of the profiles. This layback correction is reasonable when towing in straight lines and less accurate during ship turns. Most Flyer deployments thus far have been planned to reduce the number of turns and to maintain nominally straight survey lines. Should more turns be necessary, the layback correction could be improved to include ship-relative range and bearing measurements of the clump using an ultrashort baseline (USBL) acoustic system.

b. *Sensor processing*

The placement of the SBE49 within the Wire Flyer body necessitates postprocessing of the CTD data to account for the time lag associated with the length of the intake tubing and the thermal mass of the conductivity cell. Neglecting these effects would result in up-down

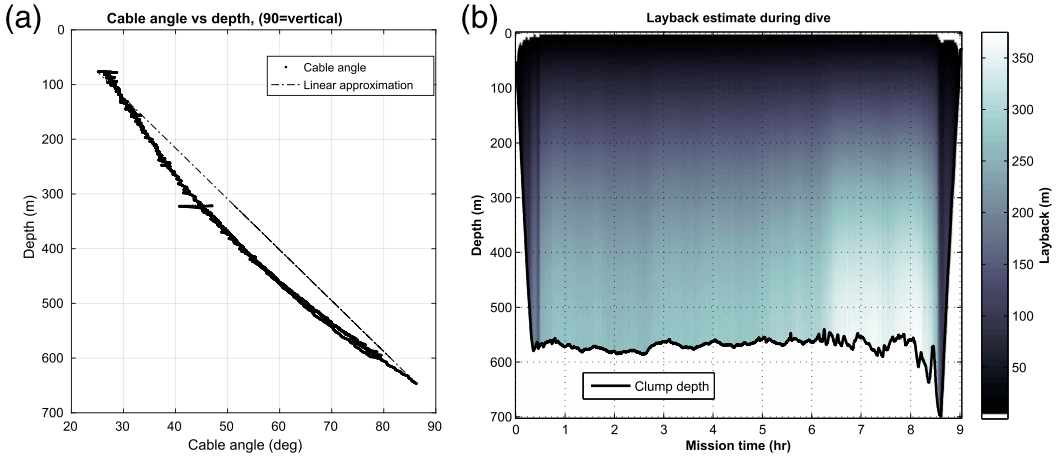

FIG. 15. (a) Example of the linear fit constrained by cable length from algorithm 1. (b) The layback estimate for a whole dive showing some variation over time. At the end of the dive the ship stopped, the clump weight started to sink deeper before being recovered, and the layback distance dropped.

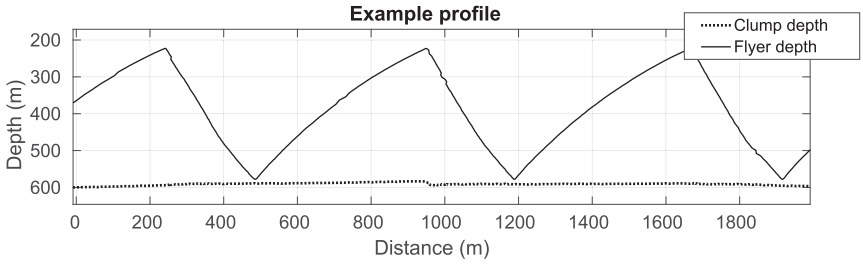

FIG. 16. Depth profiles corrected for layback and plotted with 1:1 aspect ratio.

hysteresis of temperature or salinity between sequential vehicle profiles. The flow rate of the SBE49 pump, with the CTD in its standard configuration without a length of intake and exhaust tubing, is 32 ml s^{-1} (C. Jansen, Sea-Bird Electronics, 2015, personal communication). For the approximately 0.15-m length of the intake tubing with an inside diameter of 0.635 cm, and neglecting boundary layer effects in the tube, this would suggest a pumping lag of 0.149 s or 2.38 SBE49 scans. Application of this lag to the temperature measurements (relative to the SBE49 pressure) and examination of temperature profiles from sequential upward/downward trajectories shows that this value is not sufficient to remove the vertical offsets and that the pumping lag is actually much longer.

The time lag associated with the movement of water from the intake port to the SBE49 temperature/conductivity sensors was empirically determined by comparing SBE49 temperatures to a temperature measured with an internally recording SBE56 sensor mounted on the outside of the Flyer body. The SBE56 temperature sensor has a time constant of approximately 0.5 s and was sampled at 0.5-s intervals.

To be useful for assessing the SBE49 pumping lag, the timing of the internally recording SBE56 had to be synchronized to the SBE49 time. This was done by comparing SBE56 temperature profiles on sequential upward/downward trajectories using the SBE49 pressure for the depth measurement. Assuming horizontal uniformity in temperature between sequential upward/downward trajectories, a timing difference between the SBE56 and SBE49 results in SBE56 temperature differences at the same depths on sequential trajectories. For each flyer tow, we estimated the time offset between the SBE56 and the SBE49 as the value that minimized the mean difference between SBE56 temperatures (interpolated to 0.25-dbar intervals) on sequential trajectories, averaged over all trajectories. The time offset computed in this way is accurate only to about 0.1 s (one to two scans of the 16-Hz SBE49), but it did correct for the occasional large time differences that occurred.

With the time bases of the SBE56 and SBE49 aligned, the temperature records from the two instruments were compared to determine the time lag associated with the flow through the intake tube. First, the SBE56 temperature, interpolated to the sampling times of the SBE49, was adjusted to the vertical position of the CTD intake using the known vertical speed of the flyer. Then, the time lag was determined for each upward and downward trajectory as the lag at which the correlation of the first differenced temperature signals from the two sensors was maximized. The lag values were averaged over each tow and then subsequently over all tows to produce overall averaged lag values of 13.8 $\pm$ 0.7 scans for downward trajectories and 10.3 $\pm$ 0.4 scans for upward trajectories. In processing the CTD data, these lags are applied to temperature and conductivity by advancing these variables with respect to the SBE49 pressure.

Two issues are raised by the results of the pumping lag analysis. The first is the reason for the relatively long lag in comparison with the estimate based on the flow rate of the pump mentioned above. It does not appear to be due to head loss in the intake and outlet tubing (a crude deck test of the SBE49 pump flow rate with the Flyer plumbing produced a flow rate, 29 ml s^{-1}, that was only slightly less than the flow rate provided by Sea-Bird). This suggests a dynamic effect when the vehicle is operating. The second issue with respect to the pumping lag is the significant difference between upward and downward trajectories. Examination of the individual trajectory lags as a function of wing angle and tail angle indicates that on downward trajectories, the lag becomes large when the wing and tail angles suggest that the CTD inlet/outlet ports are in the wake of the wings. The precise reason that the wake would cause the pumping lag to increase is not clear; however, the observations suggest a relationship.

Alignment of the conductivity C and temperature T measurements for minimization of salinity spiking was investigated empirically. For each downward and upward trajectory, the lagged correlation between first differenced T and C was computed. The overall mean lag of T relative to C was found to be -0.83 scans, indicating that T should be advanced in time relative to C. This value can be compared to the manufacturer's recommendation for the SBE49 of a one-scan advance

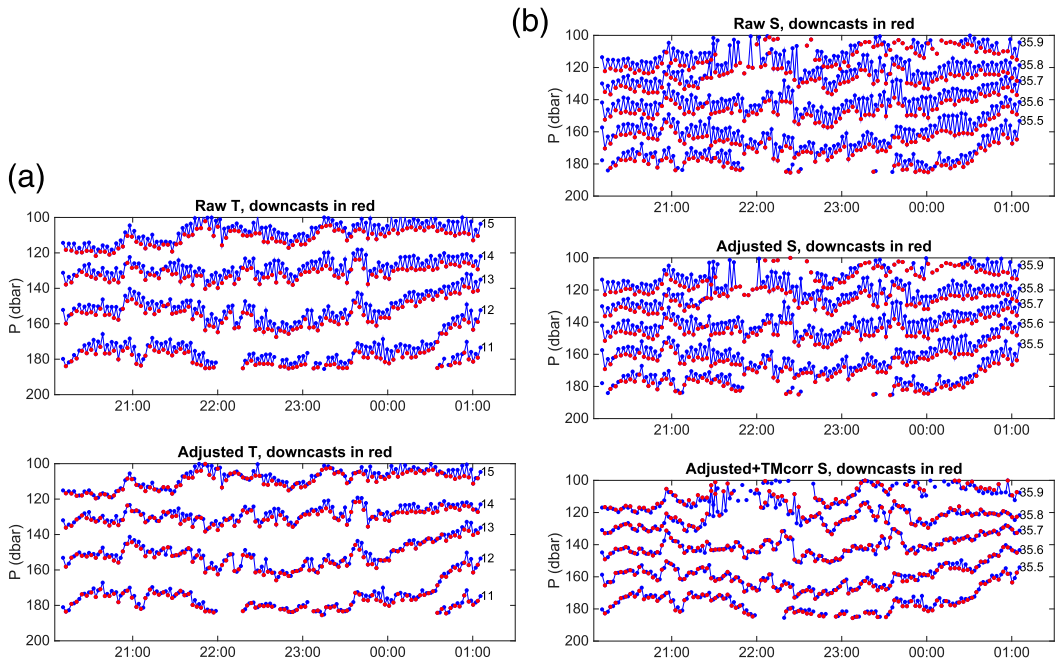

FIG. 17. (a) Isotherm depths and (b) isohaline depths as a function of time for a Wire Flyer tow during November 2014. The blue (red) dots are the values from upward (downward) profiles. The top panels are the isopleth depths using the raw CTD data. The second panel from the top shows the isopleth depths after applying the correction for the pumping lag, and for salinity the alignment of T and C. The bottom panel in (b) shows isohaline depths after applying the conductivity cell thermal mass correction.

of T. Since this advance is due to a combination of the relative response times of the T and C sensors with the latter exhibiting flow dependence, the difference likely arises from slower flushing of the conductivity cell in the Flyer SBE49.

For the SBE49, Sea-Bird recommends the use of their standard correction for the effect of the thermal mass of the conductivity cell (Lueck and Picklo 1990). Note that this corrects for mismatches between the temperature measured by the thermistor and the actual temperature of the water in the conductivity cell. It is distinct from any larger-scale thermal mass effects from the Wire Flyer vehicle itself, which would potentially affect the measured temperature and the temperature within the conductivity cell, but it would not produce anomalous salinity values.

To determine the optimum parameters for the thermal mass correction, a methodology based on that used by Morison et al. (1994) was used. Thermal mass errors give rise to two distinct types of discrepancies between downward and upward profiles. The first is an offset of salinity at a given depth (or temperature value). The second is a severe underestimation of salinity on upward profiles when entering the surface mixed layer (in a case where temperature decreases downward). This gives rise to a large density inversion within the mixed layer. The first error is quantified by computing, for each pair of profiles, the difference in salinity S within temperature bins (we expect the T–S relation between adjacent casts to be the same). The second error is assessed by computing the potential energy anomaly of the upward profile relative to the sorted (statically stable) profile [large potential energy (PE) anomalies occur when there is severe underestimation of S at the mixed layer base]. These computations are done for every upward/downward profile pair and for a range of thermal mass correction parameters [α and τ in the Lueck and Picklo (1990) formulation]. The salinity difference and PE anomalies are averaged over all casts (and in the case of salinity difference, all temperature bins) to form the two-dimensional functions $dS(\alpha, \tau)$ and $\mathrm{PE}(\alpha, \tau)$. These functions were combined into the cost function

$$\mathrm{CF} = 0.5\left[\frac{dS}{\mathrm{std}(dS)}\right] + 0.5\left[\frac{\mathrm{PE}}{\mathrm{std}(\mathrm{PE})}\right]. \qquad (1)$$

The minimum of this function was found, and the α and τ values corresponding to the minimum ($\alpha = 0.020, \tau = 13.2$) were considered the optimum correction parameters.

The effects of the corrections for pumping lag and conductivity cell thermal mass are shown in Fig. 17a for temperature and Fig. 17b for salinity. The top panels in

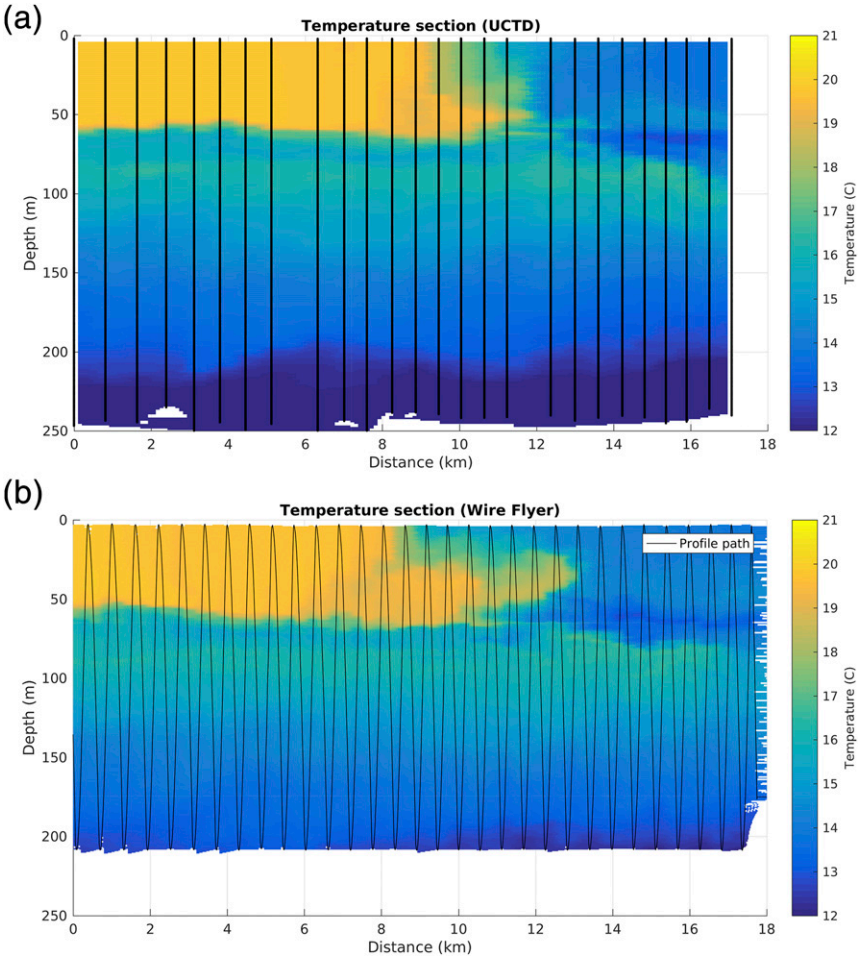

FIG. 18. Comparison between sections of UCTD and Wire Flyer tows in the same area. (a) Temperature section made with the UCTD at 4 kt. The larger gaps in the profiles at the 6- and 12-km points were caused by swapping out the probe. (b) The same section made with the Wire Flyer towed at 4 kt captures more detail. The line end points are (39.807°N, 70.063°W) and (39.818°N, 69.864°W).

these plots show isotherm and isohaline depths versus time using the raw, uncorrected T and C values. For both T and S, there is a significant oscillation corresponding to the vehicle's undulation cycle that results from the pumping lag (both T and S) as well as the conductivity cell thermal mass (S). The second panels from the top show the effect of applying the correction for pumping lag, and for salinity the alignment of T and C. The isotherm oscillations are reduced considerably. Although some reduction in the isohaline oscillations is seen, there are still significant oscillations remaining as a result of the cell thermal mass effect. Application of the cell thermal mass correction greatly reduces the amplitude of the isohaline oscillations as seen in Fig. 17b (bottom panel).

Because the auxiliary sensors such as the oxygen optode and the fluorometer do not measure pressure, the depths associated with these data streams are computed from the SBE49 pressure measurement. Since the pitch angle of the Flyer is variable, the pressure offset for the auxiliary sensors also varies with time. This time-variable offset was computed using the known horizontal and vertical locations of the SBE49 pressure port and the auxiliary sensors, and the measured vehicle pitch.

c. *Sample data*

Section plots are created using the Flyer depth and position calculated by the cable layback estimate. The sensor data are gridded at regularly spaced depth, time, or distance intervals using a Delaunay triangulation–type gridder. The gridpoint estimates are calculated as a distance-weighted linear interpolation of the values at the surrounding three vertices in a triangulation of all

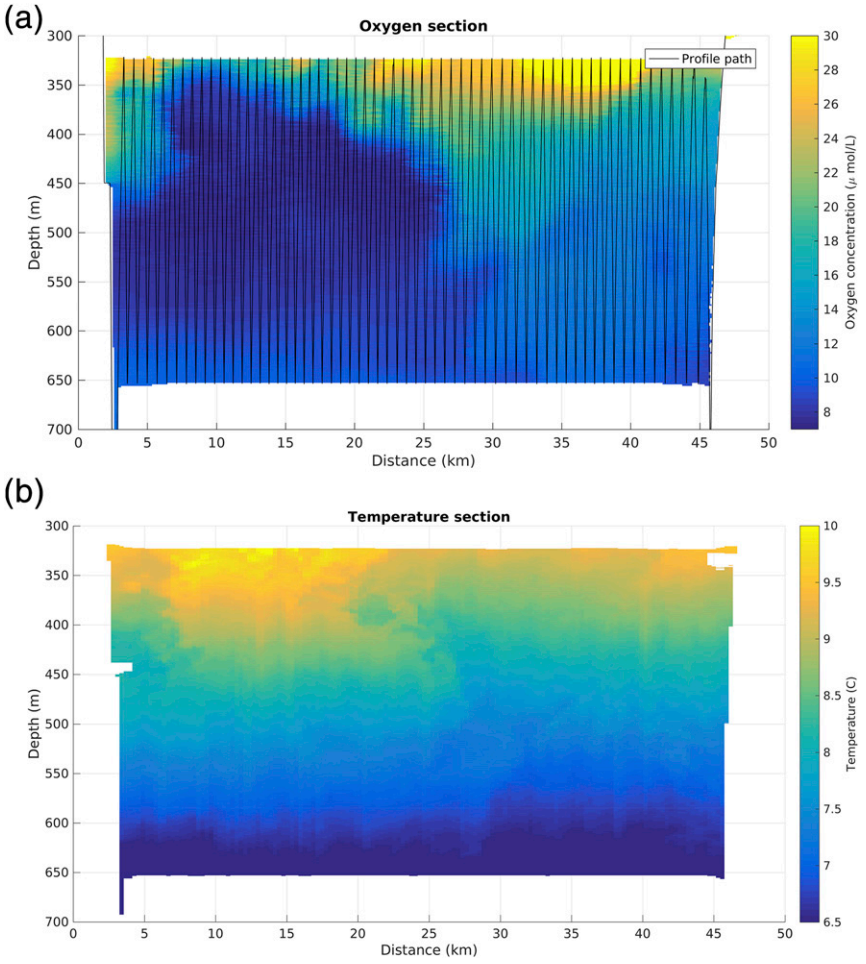

FIG. 19. Sections focusing on the oxygen minimum zone. (a) An oxygen section showing coherent structures over several kilometers. (b) The matching temperature section showing some structure that is well resolved and spatially consistent with the lower oxygen water in (a). The line end points are (21.303°N, 117.463°W) and (21.716°N, 117.597°W).

the data points. Regular grid points outside of the triangulation area or more than a specified distance from a triangle vertex are not estimated and left blank. This method of gridding is effective for retaining detail where the profile spacing is tight while avoiding excessive interpolation away from the actual vehicle trajectory. The plots shown here demonstrate the capabilities of the Wire Flyer over various depth bands from the surface down to 1000 m.

A sample temperature section to 200-m depth from the New England shelfbreak front is shown in Fig. 18. Two tows were performed along the same line to compare the Wire Flyer to a UCTD system at the same 4-kt ship speed. The UCTD section, Fig. 18a, was completed in a quickly repeating tow-yo fashion, by not recovering the probe between casts and not rewinding the line on the probe itself. The UCTD data were processed to apply the fall-rate-dependent conductivity and temperature sensor alignment and thermal mass correction that are necessary for tow-yo casts (Ullman and Hebert 2014). The Wire Flyer, Fig. 18b, was set to profile up and down at 2.0 m s^{-1}. Over this depth range, which is typical for UCTD deployments and towed undulating systems, the Flyer is able to achieve roughly double the number of UCTD profiles over a given distance at the same ship speed.

The Wire Flyer has been used on two cruises studying the oxygen minimum zone in the eastern tropical Pacific. The majority of the dives were done in the 300–700-m-depth range to capture the transitions at the top and bottom of the oxygen minimum depth. Figure 19 shows a sample section. The vehicle is able to resolve structure in the oxygen and temperature sections that is spatially correlated and changing over scales of kilometers. Maintaining this 600–800-m profile spacing at ship

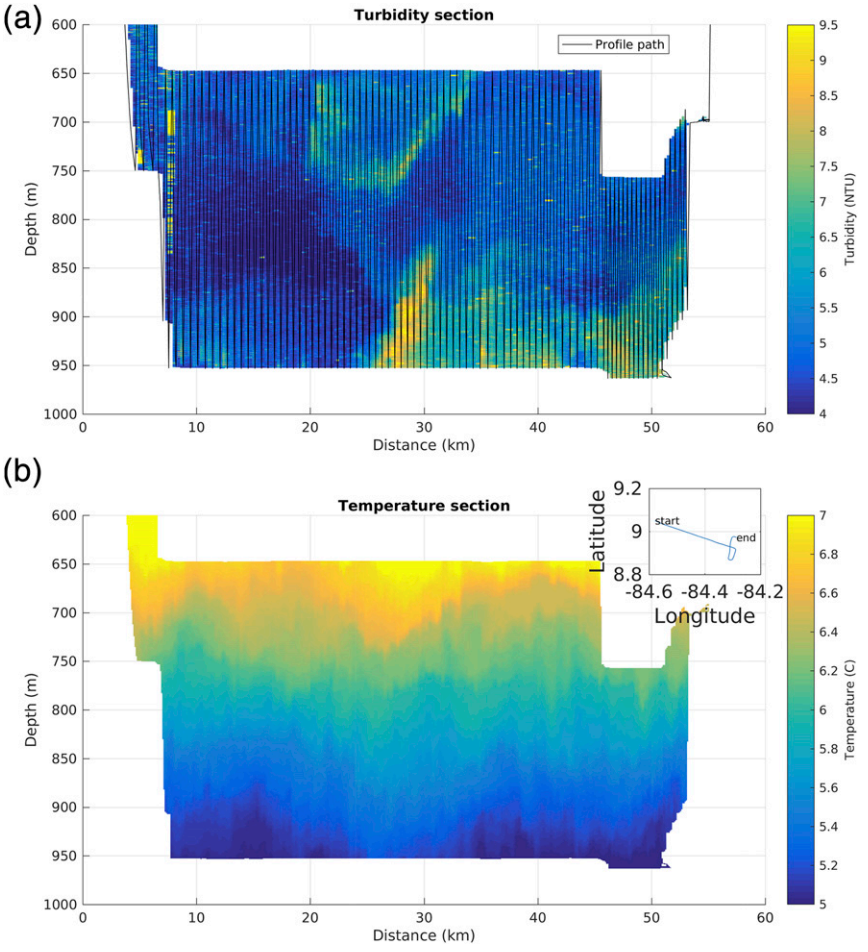

FIG. 20. Example sections collected in the vicinity of a methane seep. (a) A turbidity section showing small kilometer-scale fluctuations. (b) The matching temperature section. The seep is located at 35- and 52-km distances along the track, where it crosses over itself.

speeds of 4 kt would not be possible with existing repeat profilers and undulating bodies at this depth.

The system has also been used to look at the water column in the vicinity of seep systems down to 1000 m, which is the vehicle's current depth limit. In this case profiles were completed to within 25 m of the seafloor in an attempt to capture near-bottom temperature, turbidity, ORP, and pH anomalies. Figure 20 shows an example turbidity plot and the matching temperature field. The Wire Flyer is able to resolve coherent kilometer-scale turbidity structures that may be associated with the methane seep and would be aliased by CTD casts and sparser profiles.

In addition to deep sections, the Wire Flyer has also been used in shallow water. Figure 21 shows a section produced by rapidly profiling across the New England shelf. The vehicle was set to profile at vertical speeds of 2 and 3 m s^{-1}, with ship speeds of 4 and 5 kt. This creates a dense profile pattern that repeats approximately every 100 m. When operating in shallow water or near the clump weight, the vehicle has an adaptive turnaround behavior that starts profiles over a narrower depth band than specified and then expands the turning depths such that there is no overshoot. This can be seen in the first several cycles in Fig. 21a and again at the 17-km distance when the profile range is changed. For the last section of profiles, after the 20-km mark, the Flyer was able reach the desired velocity of 3.0 m s^{-1} at a ship speed of 5 kt. This sampling pattern is similar to what can be achieved with a UCTD or undulating tow body, and demonstrates that the vehicle can be used effectively in both deep and shallow water.

4. Conclusions

The Wire Flyer vehicle was developed to provide a detailed look at water column structure at depths that have been traditionally undersampled. The vehicle fills a niche beyond the depth capabilities of current

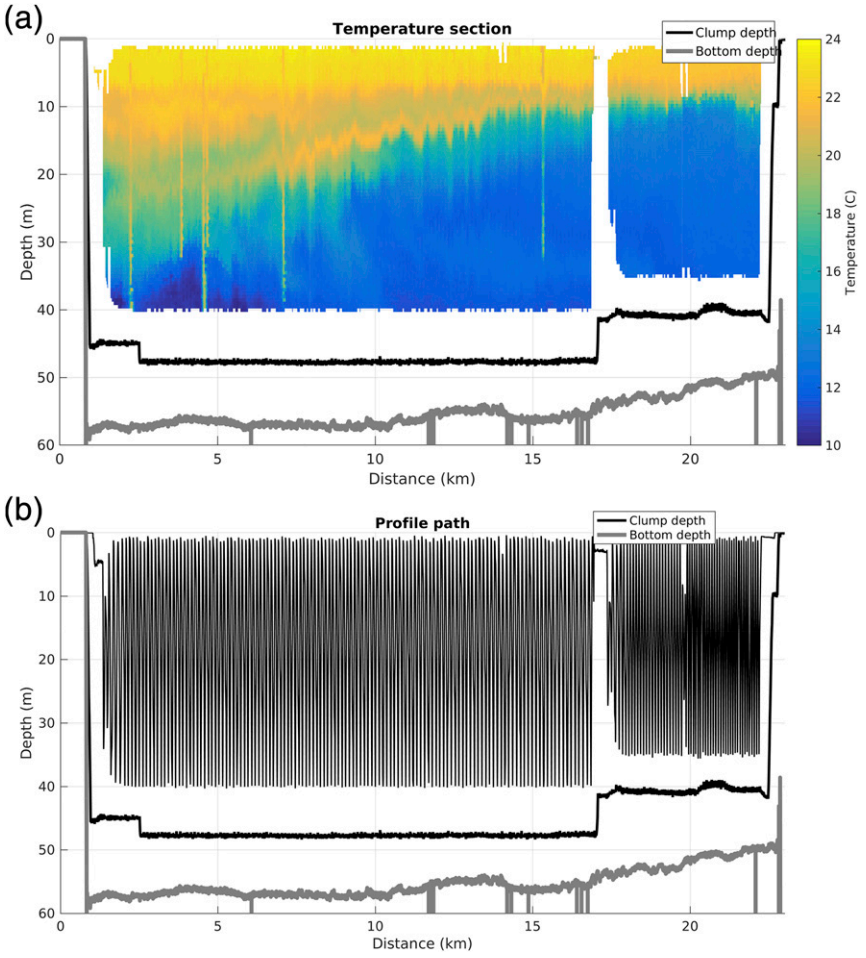

FIG. 21. A shallow northerly section created across the New England shelf during the summer, 19 Aug. (a) Temperature section showing the strong stratification becoming farther on the shelf. The five vertical streaks in the section are the result of the top of the vehicle coming out of the water and air being drawn into the CTD intake plumping. (b) The profile plot shows tight repeat profiles, with 10-m spacing. The ship speed was 4 kt for the main section and 5 kt in the later portion after the clump was raised. The line end points are (40.884°N, 71.274°W) and (41.024°N, 71.458°W).

undulating tow bodies and provides a sampling density not easily obtained with repeating underway profilers. This will provide insight into processes at the submesoscale that are otherwise difficult to observe.

In general, the vehicle is able to complete profiles at vertical speeds up to $1.75\,\mathrm{m\,s^{-1}}$ when operating in a 400-m band above the clump weight. The up and down rates are controllable and can be set by the user. Larger depth bands are possible, but it is likely the vehicle will slow down at the top of the profile and increase the cycle time between profiles. For planning Flyer deployments, it is best to assume ship speeds of 3–4 kt when the surface currents are less than 1 kt. When the surface current is greater than 1 kt, the difference in cable shape can be significant when traveling with or against the flow. In this case it is helpful to monitor the shipboard ADCP, if available, to plan surveys.

The results presented here are intended to provide an overview of the vehicle's performance envelope and show some anticipated use cases. As of mid-2018 the Flyer has completed more than 50 deployments while being used on two research cruises focusing on the oxygen minimum zone and one looking at the water column near methane seeps. Results from these projects will be presented in future publications and provide more insight into the different sensor data and the spatiotemporal sampling characteristics of the vehicle. The 3–4-kt speed range is roughly an order of magnitude faster than profiling gliders but a quarter as fast as some towed and repeat profilers. Depending on the process of interest, the resulting sections

may or may not capture the water column in a synoptic manner over submesoscale distances. This, however, is a common trade-off with all such instruments, where the profiling depth, ship speed, and horizontal resolution are typically competing parameters.

Some planned improvements to the Wire Flyer vehicle include incorporating a side-looking dual-frequency EK-80 echo sounder and moving the location of the CTD sensor. The EK-80 will provide acoustic backscatter information paired with environmental data at depths that cannot be easily reached because of the frequency attenuation limits of shipboard acoustics. The coregistered acoustic and environmental data will be used to better understand the coupling between the mesopelagic scattering layer and spatially varying oxygen concentrations. The CTD sensor will be moved to the leading edge of the vehicle to reduce the time lag and thermal mass issues related to pumping water inside the vehicle. To assist in setting the ship speed while towing, a simple flow speed sensor on the clump is being considered. This would provide an estimate of the through-water speed at depth and give the ship a better desired speed to achieve even as the speed over ground and the speed through the water vary with current and location.

Acknowledgments. Funding for the Wire Flyer has been provided by the National Science Foundation (NSF) under Grants 0728600 and 0968947. Test data shown here were also collected on NSF Projects 1459243 and 1634559. The authors are grateful for the contributions of many people who have worked with the Wire Flyer. Todd Gregory completed the detailed mechanical design. William Snyder, David Casagrande, and Kris Krasnosky developed the vehicle software, operator interface, and electrical system. Brian Amaral and Luke Logan completed masters of science theses looking at the initial hydrodynamic design and the subsequent performance evaluation. The authors are also thankful for the help provided by the crew of the R/V *Endeavor* during the test cruises at the New England shelfbreak front.

APPENDIX A

Mission Planning

Mission planning is accomplished using a simple mission script text file. The file consists of global parameters and then behavior-specific parameters and timeouts. An example is given below for a simple profiling mission. Current behaviors include fixed wing angles, constant depth control, profiling at set up and down velocities, and stair-step profiles. Any number of behaviors can be placed in a mission but typically deployments consist of fixed depth holds while the clump weight is being lowered and then profile sections between two depths. Before deploying the vehicle, missions are simulated at 10× speed using an addition program that mimics the dynamics of the vehicle and produces LCM data messages identical to those of the actual sensors. The simulation is useful for catching mistakes and accurately planning the timing of a deployment. Missions are started with a modem command or once the vehicle hits the water, as detected by the depth sensor.

```
GLOBAL
 mis_timeout 02:00:00
 enable_battery_abort 1
 enable_modem 1
 battery_cutoff 20 # % remain in battery
 max_depth 500 #meters
ENDGLOBAL
START
 start_depth 30 #delay after hitting water
ENDSTART
HOLD_DEPTH
 leg_timeout 15:00
 depth 10 #m
ENDHOLD_DEPTH
ADAPT_VEL_PROFILE
 leg_timeout 45:00
 u_vel 2.00 #m/sec up velocity
 d_vel 1.75 #m/sec down velocity
 u_depth 50 #upper depth
 l_depth 250 #lower depth
 stall_comp 15 #stall prevention angle
ENDADAPT_VEL_PROFILE
ADAPT_VEL_PROFILE
 leg_timeout 45:00
 u_vel 1.750 #m/sec up velocity
 d_vel 1.750 #m/sec down velocity
 u_depth 200 #upper depth
 l_depth 450 #lower depth
 stall_comp 15 #stall prevention angle
ENDADAPT_VEL_PROFILE
HOME
 wing_ang 20 #wing angle for recovery
ENDHOME
```

APPENDIX B

Layback Calculation

A linear relation can be used to estimate the cable angle as

$$\theta = a \times z + b, \tag{B1}$$

where a is a change in angle with depth, b is the cable angle at the surface, and z is the depth. Both a and b can be estimated iteratively using the measured cable payout and clump depth as constraints. Algorithm 1 is used in post-processing to step though a dive and to produce an estimate of the cable layback to locate the vehicle behind the ship. The main assumption is that the cable shape is relatively constant over short time intervals of a few minutes. The method iteratively determines the constants a and b that describe the cable angle and produces a cable length that matches the recorded winch payout.

Algorithm 1 Length constrained cable layback calculation

Break dive into time increments, typically 3 min

Set angle at clump, θ_c, typically, 88° from horizontal

Set depth increment dz, typically 5 m

Set an initial value for b, typically 80°

for each time increment during the dive **do**

Set c_{actual} to the actual cable length to from the winch measurement

Set z_c to the measured clump depth

Create a vector of depths Z, from 0 to z_c, spaced at increments dz

while $|c_{\text{actual}} - c_{\text{estimate}}| < 0.1$ meters **do**

$a = (\theta_c - b)/z_c$

Calculate cable length c_{estimate} using angle estimates along the cable from $\theta = a \cdot Z + b$

Adjust angle offset, $b = b \cdot \dfrac{c_{\text{estimate}}}{c_{\text{actual}}}$

end while

Calculate the laybacks at the time increment for all depths in Z

end for

Use calculated laybacks at time increments to interpolate a layback for all depths and times along the vehicle path

REFERENCES

Allen, V., J. Cornell, M. Moore, N. Crisp, and J. Dunning, 2002: Operational oceanography using the new SeaSoar ocean undulator. *Sea Technol.*, **43** (4), 35–40.

Amaral, B., 2012: The hydrodynamic optimization of a cable-flying vehicle. M.S. thesis, Ocean Engineering Dept., University of Rhode Island, 127 pp.

Baker, E., and H. B. Milburn, 1997: MAPR: A new instrument for hydrothermal plume mapping. *Ridge Events*, **8** (1), 23–25.

——, and C. German, 2004: On the global distribution of hydrothermal vent fields. *Mid-Ocean Ridges: Hydrothermal Interactions between the Lithosphere and Oceans*, *Geophys. Monogr.*, Vol. 148, 245–266, https://doi.org/10.1029/148GM10.

Beaudoin, J., S. Smyth, A. Furlong, H. Floc'h, and X. Lurton, 2011: Streamlining sound speed profile pre-processing: Case studies and field trials. *Proc. U.S. Hydrographic Conf. (US HYDRO)*, 811. https://scholars.unh.edu/ccom/811, Tampa, FL, Hydrographic Society of America, 19 pp.

Cole, S. T., D. L. Rudnick, and J. A. Colosi, 2010: Seasonal evolution of upper-ocean horizontal structure and the remnant mixed layer. *J. Geophys. Res.*, **115**, C04012, https://doi.org/10.1029/2009JC005654.

Dickey, T. D., E. C. Itsweire, M. Moline, and M. J. Perry, 2008: Introduction to the *Limnology and Oceanography* special issue on autonomous and Lagrangian platforms and sensors (ALPS). *Limnol. Oceanogr.*, **53**, 2057–2061, https://doi.org/10.4319/lo.2008.53.5_part_2.2057.

Furlong, A., J. Osler, H. Christian, D. Cunningham, and S. Pecknold, 2006: The Moving Vessel Profiler (MVP)—A rapid environmental assessment tool for the collection of water column profiles and sediment classifications. *Proc. Undersea Defence Technology Pacific Conf.*, San Diego, CA, 1–13, https://apps.dtic.mil/dtic/tr/fulltext/u2/1005165.pdf.

Gobat, J. I., and M. A. Grosenbaugh, 2000: WHOI Cable v2.0: Time domain numerical simulation of moored and towed oceanographic systems. Woods Hole Oceanographic Institution Tech. Rep. WHOI-2000-08, 89 pp.

Hainbucher, D., V. Cardin, G. Siena, U. Hübner, M. Moritz, U. Drübbisch, and F. Basan, 2015: Hydrography in the Mediterranean Sea during a cruise with RV *Poseidon* in April 2014. *Earth Syst. Sci. Data*, **7**, 231–237, https://doi.org/10.5194/essd-7-231-2015.

Herman, A. W., B. Beanlands, M. Chin-Yee, A. Furlong, J. Snow, S. Young, and T. Phillips, 1998: The Moving Vessel Profiler (MVP): In-situ sampling of plankton and physical parameters at 12 kts and the integration of a new laser/optical plankton counter. *Oceanology*, **102**, 123–135.

Hobson, B. W., J. G. Bellingham, B. Kieft, R. McEwen, M. Godin, and Y. Zhang, 2012: Tethys-class long range AUVs—Extending the endurance of propeller-driven cruising AUVs from days to weeks. *2012 IEEE/OES Autonomous Underwater Vehicles (AUV)*, IEEE, 8 pp., https://doi.org/10.1109/AUV.2012.6380735.

Huang, A. S., E. Olson, and D. C. Moore, 2010: LCM: Lightweight communications and marshalling. *2010 IEEE/RSJ International Conference on Intelligent Robots and Systems (IROS)*, IEEE, 4057–4062, https://doi.org/10.1109/IROS.2010.5649358.

Itoh, S., H. Kaneko, M. Ishizu, D. Yanagimoto, T. Okunishi, H. Nishigaki, and K. Tanaka, 2016: Fine-scale structure and mixing across the front between the Tsugaru Warm and Oyashio Currents in summer along the Sanriku Coast, east of Japan. *J. Oceanogr.*, **72**, 23–37, https://doi.org/10.1007/s10872-015-0320-6.

Janout, M. A., T. J. Weingartner, S. R. Okkonen, T. E. Whitledge, and D. L. Musgrave, 2009: Some characteristics of Yakutat Eddies propagating along the continental slope of the northern Gulf of Alaska. *Deep-Sea Res. II*, **56**, 2444–2459, https://doi.org/10.1016/j.dsr2.2009.02.006.

Kunze, E., J. M. Klymak, R.-C. Lien, R. Ferrari, C. M. Lee, M. A. Sundermeyer, and L. Goodman, 2015: Submesoscale water-mass spectra in the Sargasso Sea. *J. Phys. Oceanogr.*, **45**, 1325–1338, https://doi.org/10.1175/JPO-D-14-0108.1.

Logan, L. A., 2014: Performance analysis of an underwater wire flying profiling vehicle. M.S. thesis, Dept. of Oceanography, University of Rhode Island, 49 pp.

Lueck, R. G., and J. J. Picklo, 1990: Thermal inertia of conductivity cells: Observations with a Sea-Bird cell. *J. Atmos. Oceanic Technol.*, **7**, 756–768, https://doi.org/10.1175/1520-0426(1990)007<0756:TIOCCO>2.0.CO;2.

Moore, C. M., S. Seeyave, A. E. Hickman, J. T. Allen, M. I. Lucas, H. Planquette, R. T. Pollard, and A. J. Poulton, 2007: Iron–light interactions during the CROZet natural iron bloom and export experiment (CROZEX) I: Phytoplankton growth and photophysiology. *Deep-Sea Res. II*, **54**, 2045–2065, https://doi.org/10.1016/j.dsr2.2007.06.011.

Morison, J., R. Andersen, N. Larson, E. D'Asaro, and T. Boyd, 1994: The correction for thermal-lag effects in Sea-Bird CTD data. *J. Atmos. Oceanic Technol.*, **11**, 1151–1164, https://doi.org/10.1175/1520-0426(1994)011<1151:TCFTLE>2.0.CO;2.

Pichon, A., Y. Morel, R. Baraille, and L. Quaresma, 2013: Internal tide interactions in the Bay of Biscay: Observations and modelling. *J. Mar. Syst.*, **109–110**, S26–S44, https://doi.org/10.1016/j.jmarsys.2011.07.003.

Pollard, R., 1986: Frontal surveys with a towed profiling conductivity/temperature/depth measurement package (SeaSoar). *Nature*, **323**, 433–435, https://doi.org/10.1038/323433a0.

Ramp, S. R., Y. J. Yang, D. B. Reeder, and F. L. Bahr, 2012: Observations of a mode-2 nonlinear internal wave on the northern Heng-Chun Ridge south of Taiwan. *J. Geophys. Res.*, **117**, C03043, https://doi.org/10.1029/2011JC007662.

Roman, C., and D. Hebert, 2011: Concept tests for a new wire flying vehicle designed to achieve high horizontal resolution profiling in deep water. *J. Atmos. Oceanic Technol.*, **28**, 1657–1671, https://doi.org/10.1175/JTECH-D-10-05040.1.

Rudnick, D. L., 2016: Ocean research enabled by underwater gliders. *Annu. Rev. Mar. Sci.*, **8**, 519–541, https://doi.org/10.1146/annurev-marine-122414-033913.

——, and J. Klinke, 2007: The Underway Conductivity–Temperature–Depth instrument. *J. Atmos. Oceanic Technol.*, **24**, 1910–1923, https://doi.org/10.1175/JTECH2100.1.

——, and S. T. Cole, 2011: On sampling the ocean using underwater gliders. *J. Geophys. Res.*, **116**, C08010, https://doi.org/10.1029/2010JC006849.

——, D. Costa, K. Johnson, C. Lee, and M.-L. Timmermans, Eds., 2018: ALPS II—Autonomous and Lagrangian platforms and sensors: A report of the ALPS II Workshop. ALPS Group, 66 pp., https://alps-ocean.us/pdfs/ALPS-II.pdf.

Sellschopp, J., 1997: A towed CTD chain for two dimensional high resolution hydrography. *Deep-Sea Res. I*, **44**, 147–165, https://doi.org/10.1016/S0967-0637(96)00087-8.

——, and Coauthors, 2006: Direct observations of a medium-intensity inflow into the Baltic Sea. *Cont. Shelf Res.*, **26**, 2393–2414, https://doi.org/10.1016/j.csr.2006.07.004.

Ullman, D. S., and D. Hebert, 2014: Processing of underway CTD data. *J. Atmos. Oceanic Technol.*, **31**, 984–998, https://doi.org/10.1175/JTECH-D-13-00200.1.

Van Uffelen, L. J., P. F. Worcester, M. A. Dzieciuch, D. L. Rudnick, and J. A. Colosi, 2010: Effects of upper ocean sound-speed structure on deep acoustic shadow-zone arrivals at 500- and 1000-km range. *J. Acoust. Soc. Amer.*, **127**, 2169–2181, https://doi.org/10.1121/1.3292948.

Zhang, Y., R. S. McEwen, J. P. Ryan, and J. G. Bellingham, 2010: Design and tests of an adaptive triggering method for capturing peak samples in a thin phytoplankton layer by an autonomous underwater vehicle. *IEEE J. Oceanic Eng.*, **35**, 785–79, https://doi.org/10.1109/JOE.2010.2081031.